Space-based surface change detection with differential Synthetic-Aperture Radar (SAR) Interferometry: potentialities and preliminary investigations

Antonio Vettore[1], Salvatore Ponte[2], Nicola Crocetto[3]

[1]DAUR, University of Padua, Via Marzolo, 9 – 35131 Padua, Italy

[2]Dept. Aerospace Engineering, Second University of Naples, Via Roma, 29 - I-81301 Aversa (CE), Italy

[3]Dept. Civil Engineering, Second University of Naples, Via Roma, 29 - I-81301 Aversa (CE), Italy

ABSTRACT

The capability of measuring small crustal deformation by means of differential Synthetic Aperture Radar (SAR) interferometry (DIFSAR) is investigated in this work. After outlining the mathematical background inherent to the principles of differential SAR interferometry and showing the potential and limits of the information content of spaceborne DIFSAR data, the analysis of the impact of this technique is carried out on some interferometric couples gathered in 1996 by the ERS-1/ERS-2 (European Remote Sensing Satellite) tandem mission. The imaged scene is a portion of the Sannio-Matese mountainous area (Southern Italy). Suitable interferometric couples are processed and analyzed in order to show potentialities of detecting surface deformation by means of DIFSAR data, and derive qualitative information on the relationship between DIFSAR-based change detection and the time scale of crustal dynamics, by investigating the effectiveness of the technique as a function of the scene coherence. Preliminary results confirm the feasibility of the technique, even at the cost of sophisticated processing and careful error analysis.

Keywords: Synthetic Aperture Radar, Interferometry, Change detection.

1. Introduction

Known and theorised since 1989 (Gabriel *et al.* 1989), the Differential Interferometric Synthetic Aperture Radar (DIFSAR) technique has recently become of paramount interest in detecting surface changes at centimetric level (Werner *et al.* 1992, Prati *et al.* 1993, Franceschetti and Lanari 1999), adding a new dimension to geospatial data processing. Spaceborne DIFSAR data are becoming appealing thanks to the advantage of global and rapid coverage, ease of accessibility, and revisiting capabilities. The relatively large amount of data acquired by existing or past spaceborne SAR sensors like ERS-1, ERS-2, JERS-1 (Japanese Earth Resources Satellite), SIR-C/X-SAR (Spaceborne Imaging Radar-C, X-band Synthetic Aperture Radar), and the Canadian RADARSAT, gives opportunities for a fairly complete assessment of DIFSAR potential for crustal dynamics applications (see Rosen *et al.* 2000, Sec. V.B for a thorough list of applications). On the other hand, more control over the repetition interval is assured by airborne platforms, which can accommodate fast surface changes and track rapidly evolving phenomena such as landslides and floods. Moreover, the availability of low-cost Global Positioning System (GPS) real-time measurements of the platform state vector (position, velocity, acceleration, attitude) improves dramatically the flight track knowledge and control, Small displacements of the order of the wavelength used (in the microwave region) for acquisition of three SAR images of an area are potentially feasible, and a comprehensive review study has been recently published (Massonnet and Feigl 2000). Table 1 shows a comparison between DIFSAR potentialities in measuring subsidence phenomena and some more conventional methods, based on extensometers and GPS.

Table 1. Comparison between DIFSAR-based displacement detection and some other common techniques.

Technique	Displacement component	Accuracy	Achievable spatial information	Scale
Borehole extensometer	Vertical	1 mm	<5 samples	Point
Horizontal extensometer	Horizontal	10^{-4}-0.3 mm	1-10 samples	Line
GPS	Vector	5 mm (horizontal) 10-30 mm (vertical)	10-100 samples	Geodetic network
DIFSAR	Along line of sight	<20 mm	10^5-10^7	Regional (typical pixel resolution: 30-60 m)

Nevertheless, crustal movement detection rely heavily on the quantitative changes of the scattering mechanisms of the imaged area. These scattering changes can be related to some types of displacement (for example, fault movements, landslides, glacier flowing, urban subsidence, volcanic deformations, etc.) when a coherent large-scale surface change is observed along several adjacent pixels (Vadon and Sigmundsson 1997), but backscatter variations can be due to temporal and spatial, or baseline, decorrelation effects as well. Generally speaking, therefore, DIFSAR data (and their usefulness) appear to be strictly related to terrain morphology and land use. Noise sources and critical values of some

parameters (e.g. interferometric baseline components) have to be taken into account for effective application of the technique in handling geographic and remote sensing data for risk assessment and advanced survey techniques.

This paper presents a feasibility study of the DIFSAR technique for retrieval of ground displacement at sub-wavelength level by using spaceborne data. The mathematical treatment of the topic is outlined in order to identify the observables and the error sources, and a case study is presented, illustrating preliminary results obtained by using ERS-1/ERS-2 tandem data (C-band radar images, carrier frequency 5.3 GHz), aimed at monitoring and forecasting small crustal deformations and tectonic movements in the area of the Matese Chain (Campano-Molisano Apennines, Southern Italy), known as one of the most seismically active segments of the Apennine chain (Siro and Slejko 1989, Barbano *et al.*, 1989). Results on interferometric SAR processing, coherence analysis and multiple-pass image analysis are presented, in order to assess the feasibility of DIFSAR techniques on the test area. Concluding remarks describe the future steps of the research activity.

2. Differential SAR Interferometry: mathematical background

Small-scale motion of the surface illuminated by successive radar observations induces an additional contribution to the interferometric phase, by causing coherent phase shifts (in the case of locally uniform motion of the ground) or decorrelating homologous pixels due to one-dimensional changes along the radar line of sight. The estimate of the displacement Δz with the DINSAR technique gives a scalar quantity. If other SAR interferometric phase maps can be acquired from other (non parallel) directions and different aspect angles, surface motion can be entirely recovered by resolving the displacement observations into the vector components of $\mathbf{\Delta z}$. In spaceborne SAR systems, this is typically achieved by exploiting ascending and descending passes of the sensor over the illuminated scene. In this respect, DIFSAR-based change detection differs from the intrinsecally vectorial displacements achievable with GPS real-time kinematic (RTK) measurements. On the other hand, surface changes are detected with large spatial coverage, rather than in a local fashion, typical of GPS-based geodetic surveys (Tab. 1), and large spatial density, i.e. large number of samples per survey.

In this section a mathematical model for relating ground displacement to double-difference interferograms is derived, assuming flat Earth geometry, and three serial observations of a scene, made from three locations separated by baselines B_1, B_2 and B_3 respectively.

2.1 Ground displacement from INSAR data

Fig. 1 shows the observation geometry. It is assumed that a change Δz is observable in correspondence of the third passage of the sensor, whereas the observations from locations A and B may derive from two passage of the same spaceborne SAR sensor in different times (two-pass interferometry) or from simultaneous acquisition by a spaceborne SAR interferometer (single-pass interferometry), without losing generality. For example, Δz could derive from a short-time displacement due to an earthquake, and two spaceborne interferometric couples could be available before and after the seismic event.
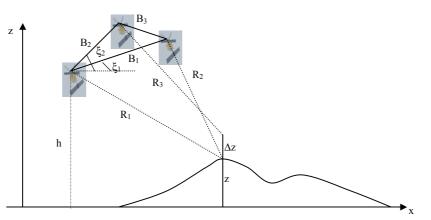

Fig. 1. Observation geometry for multiple-pass SAR interferometry. The SAR antennas are located in the positions A, B and C.

Obviously, the time scale over which the displacement is sensed must be in agreement with the geophysical nature of the phenomenon: a "temporal baseline" of few days could be appropriate for monitoring abrupt changes in higly correlated areas, but inadequate for monitoring "fast" surface changes as in ocean currents mapping. Furthermore, long temporal baselines appear suitable for monitoring slow phenomena (subsidence, or bradisismic events), as far as the scene exhibits favourable characteristics, in terms of coherence, as it will be clarified later in Sec. 2.2. For typical spaceborne geometries, the B_i (i=1,2,3) are of the order of 1 km, and the slant ranges vary from 500 to 1000 km.Given

the radar system wavelength λ, the observables (phase differences) related to the first interferometric couple (antennas A and B) and the second (antennas A and C) are given by:

$$\Delta\varphi_{AB} = \frac{4\pi}{\lambda}(R_1 - R_2); \quad \Delta\varphi_{AC} = \frac{4\pi}{\lambda}(R_1 - R_3) \tag{1}$$

where R_1, R_2 and R_3 are the slant ranges to the imaged object. Expressions of R_2 and R_3 as a function of the baselines can be easily derived from the geometry of Fig. 1. Denoting the look angle with ϑ, the sensor height and the surface height with h and z respectively, and the baseline tilt angles with respect to the horizontal with ξ_1 and ξ_2, using straightforward trigonometry, we get:

$$R_2 = \sqrt{(h-z)^2 + R_1^2 \sin^2\vartheta + 2B_1(h-z)\sin\xi_1 + B_1^2\cos^2\xi_1 - 2R_1B_1\sin\vartheta\cos\xi_1 + B_1^2\sin^2\xi_1} =$$
$$= R_1\sqrt{1 - \frac{2B_1}{R_1}\left(\sin\vartheta\cos\xi_1 - \frac{h-z}{R_1}\sin\xi_1\right) + \frac{B_1^2}{R_1^2}} \tag{2}$$

which reduces, noting that $(h-z)/R_1 = \cos\vartheta$ and using a first-order Taylor expansion, to an expression which puts in evidence the dependence of the slant range on the baseline component parallel to the look direction, $B_\parallel$, defined as $B\sin(\vartheta-\xi)$:

$$R_2 \cong R_1 - B_1\sin(\vartheta-\xi_1) + \frac{B_1^2}{2R_1} = R_1 - B_{1\parallel} + \frac{B_1^2}{2R_1} \tag{3}$$

The term $B_1^2/2R_1$ is usually neglected in simplified treatments of the topic (for example, Madsen and Zebker 1998), representing an overall bias of the order of 1 cm for spaceborne sensors. Nevertheless, when relating the range to the phase measurement, centimeter-value wavelength make such a bias not negligible (e.g. for ERS, with $\lambda \cong 5$ cm, the corresponding phase contribution of $B_1^2/2R_1$ is of the order of 1 radian).

A similar expression can be derived for R_3 when there is no surface change (i.e. $\Delta z = 0$), and the phase change between two SAR acquisitions is only due to the topography of the illuminated scene (i.e. z):

$$R_3^0 \cong R_1 - B_2\sin(\vartheta-\xi_2) + \frac{B_2^2}{2R_1} = R_1 - B_{2\parallel} + \frac{B_2^2}{2R_1} \tag{4}$$

whereas in the presence of a vertical displacement Δz, whose component along the radar line of sight is $\Delta z\cos\vartheta$, we have an additive phase term. The expression of R_3 when $\Delta z \neq 0$ becomes therefore:

$$R_3^{\Delta z} = \sqrt{(h-z)^2 + (B_2\sin\xi_2 - \Delta z)^2 + 2(h-z)(B_2\sin\xi_2 - \Delta z) + R_1^2\sin^2\vartheta + B_2^2\cos^2\xi_2 - 2R_1B_2\sin\vartheta\cos\xi_2} =$$
$$= R_1\sqrt{1 - \frac{2B_2}{R_1}\left(\sin\vartheta\cos\xi_2 - \frac{h-z}{R_1}\sin\xi_2\right) + \frac{B_2^2}{R_1^2} + \frac{\Delta z^2}{R_1^2} - \left(\frac{2B_2}{R_1^2}\sin\xi_2 + \frac{2(h-z)}{R_1^2}\right)\Delta z} \tag{5}$$

which reduces to:

$$R_3^{\Delta z} \cong R_1 - B_2\sin(\vartheta-\xi_2) + \frac{B_2^2}{2R_1} - \Delta z\left(\cos\vartheta + \frac{B_2}{R_1}\sin\xi_2\right) + \frac{\Delta z^2}{2R_1} = R_3^0 - \Delta z\left(\cos\vartheta + \frac{B_2}{R_1}\sin\xi_2\right) + \frac{\Delta z^2}{2R_1} \tag{6}$$

expanding in a first-order Taylor series and using Eq. (4). We got final expressions for $\Delta\varphi_{AB}$ and $\Delta\varphi_{AC}$ with no vertical displacement ($\Delta\varphi_{AC}^0$) and with surface displacement ($\Delta\varphi_{AC}^{\Delta z}$):

$$\Delta\varphi_{AB} = \frac{4\pi}{\lambda}\left(B_{1\parallel} - \frac{B_1^2}{2R_1}\right) \tag{7}$$

$$\Delta\varphi_{AC}^0 = \frac{4\pi}{\lambda}\left(B_{2\parallel} - \frac{B_2^2}{2R_1}\right) \tag{8}$$

$$\Delta\varphi_{AC}^{\Delta z} = \frac{4\pi}{\lambda}\left[B_{2\parallel} - \frac{B_2^2}{2R_1} + \Delta z\left(\cos\vartheta + \frac{B_2}{R_1}\sin\xi_2\right)\right] = \Delta\varphi_{AC}^0 + \Delta z\left(\cos\vartheta + \frac{B_2}{R_1}\sin\xi_2\right) \tag{9}$$

having neglected (since $\Delta z << R_1$) in Eq. (9) the term $\Delta z^2/2R_1$. Eq. (9) allows us to distinguish a contribution $\Delta\varphi_{AC}^0$ to the phase difference due to the scene topography (this contribution would be equal to 0 if $B_2=0$, i.e. if the third antenna passed over the same location as the first one), and a contribution assignable to the displacement component parallel to the look direction, usually referred to as line-of-sight (LOS) displacement (assuming $B_2/R_1 << 1$, this is the only component of the contribution). The "double-difference operator" $\Delta\Phi$, i.e. the difference of the phase differences, defined as $\Delta\varphi_{AC}^{\Delta z} - \Delta\varphi_{AB}$, relates the observables (phase differences) with the quantity being estimated, that is, Δz:

$$\Delta\Phi = \frac{4\pi}{\lambda}\left[B_2\sin(\vartheta-\xi_2) - B_1\sin(\vartheta-\xi_1) - \frac{B_2^2 - B_1^2}{2R_1} + \Delta z\cos\vartheta + \Delta z\frac{B_2}{R_1}\sin\xi_2\right] = \Delta\Phi^0 + \frac{4\pi}{\lambda}\cos\vartheta\Delta z \qquad (10)$$

where the last addend involving Δz has been neglected, being usually $B_2 << R_1$. It has to be stressed that ground displacements along the slant range direction can cause 2-π phase differences when they are of the order of $\lambda/2$, which is few centimeters in the microwave region, whereas the sensitivity of an interferogram to the topography (see Eqs. (7) and (8)) is much smaller: since $R_1=(h-z)\cos\vartheta$, a change in z of the order of R_1/B (of the order of 4000 in typical spaceborne geometries, with $R_1=800$ km and $B=200$ m) gives one-cycle phase difference. Finally:

$$\Delta z = \frac{\lambda}{4\pi}\frac{\Delta\Phi - \Delta\Phi^0}{\cos\vartheta} \qquad (11)$$

This formulation implies a-priori knowledge of the topographic characteristic of each point of the imaged scene, in order to evaluate the look angle ϑ and remove the phase term due to the topography only: for example, Massonnet *et al* (1996) used a preexisting Digital Elevation Model (DEM) in the Mojave Desert (USA) to measure coseismic effects by means of DIFSAR data. An alternative approach is the solution of the "classic SAR interferometry problem" (Crocetto and Ponte 2001), i.e. derivation of the topographic map of the area by using interferometric data. The latter approach requires four processing phases, namely:

1. Co-registration of the conventional complex SAR images;
2. Formation of the interferogram, i.e. multiplying one pixel in the first image by the complex conjugate homologous pixel in the second (co-registered) image;
3. Phase unwrapping, i.e. adding the appropriate number of 2π's to the measured image in order to take account of the distances R_1 and R_2;
4. Reconstruction of the topography of the scene (DEM evaluation).

2.2 Sensitivity analysis and noise sources of differential INSAR measurements

Assessing the relative sensitivity of the phase measurements to the topographic characteristics of the illuminated area and to the displacement between successive passes as well is a crucial issue to be addressed, since the accuracy of the knowledge of z (i.e. the DEM accuracy, typically 20-50 m, see for example Moccia *et al.* 1994) may be insufficient for a good estimate of Δz. Generally (Gabriel *et al.* 1989) the sensitivity of interferometric SAR data to the parameters being estimated depends on the observation geometry (ϑ and the baseline tilt angles, or $B_{||}$) and on the radar system phase noise, which in turn is related to the signal-to-noise ratio (SNR, Zebker *et al.* 1994). SNRs of at least 10 dB guarantee system phase noise of less than 10 degrees (Zebker and Villasenor 1992).

We begin to estimate the sensitivity of interferometric phase to the height z of the scene. Since $z=h-R_1\cos\vartheta$ (see Fig. 1), $dz=R_1\sin\vartheta d\vartheta$. From Eq. (4), and remembering that the phase contribution of the pixel at a slant range R_3 is given by $4\pi R_3/\lambda$, we get:

$$d\varphi_{R_3^0} = \frac{4\pi}{\lambda}B_2\cos(\vartheta-\xi_2)d\vartheta \qquad (12)$$

and therefore:

$$\frac{d\varphi_{R_3^0}}{dz} = \frac{4\pi}{\lambda}\frac{B_2}{R_2}\frac{\cos(\vartheta-\xi_2)}{\sin\vartheta} \qquad (13)$$

As far as the sensitivity of φ to the displacement Δz is concerned, using Eq. (6) and neglecting the Δz^2-term, we get:

$$d\varphi_{R_3^{\Delta z}} = -\frac{4\pi}{\lambda}\left(\cos\vartheta + \frac{B_2}{R_1}\sin\xi_2\right)dz \cong -\frac{4\pi}{\lambda}\cos\vartheta dz \quad \Rightarrow \quad \frac{d\varphi_{R_3^{\Delta z}}}{dz} = -\frac{4\pi}{\lambda}\cos\vartheta \qquad (14)$$

since B_i/R_i, for spaceborne geometries, is typically of the order of 10^{-3}. Analyzing Eqs. (13) and (14), it is clearly deduced that a change in topography is much less influent than a surface displacement. Assuming for example $\vartheta=30°$,

$\xi=10°$, R=800 km, B=100 m, $\lambda=0.05$ m (typical ERS parameters, C-band), a 1-meter change in topography would induce a change of about 4 degrees in the phase measurement (below the measurement phase noise, typically of 10-20 degrees), whereas the same change in surface displacement would induce an absolute phase term more than 3500 times higher. Therefore, the measurement of centimeter-level ground displacement would require an accuracy of topographic data of the order of $3500*10^{-2}$, i.e. ±35 m rms vertical errors in the interferometric DEM.

The main sources of interferogram phase noise are temporal and spatial decorrelation effects, due to the existence of spatial as well as temporal baselines in the DIFSAR technique. Spatial decorrelation effects, due to different looking directions of the same spatial resolution cell (not negligible when dealing with two-pass interferometry) increase as the baseline component orthogonal to the LOS increases (Franceschetti and Lanari 1999). Temporal decorrelation (Zebker and Villsenor 1992) is unavoidable in DIFSAR applications. The phase change contribution attributable to a surface displacement is obviously fundamental for estimating Δz, but additional temporal coherence loss can be due to weather changes as well as backscattering changes due to the changed electromagneteic properties of the imaged scene. It is therefore crucial to "tune" the available temporal baseline to the typical timescales of the crustal dynamics being detected (quick translations of the surface, like in earthquakes, or slow glacier motion, for example). The positive aspect of temporal decorrelation is that areas affected by phase noise can be identified with typical classification algorithms, obtaining radiometric classes in principle associatable with information classes (e.g. high decorrelation=forested terrain, low decorrelation=arid or urban regions, etc.). DIFSAR data, therefore, relying heavily on quantitative changes of the scattering mechanisms of the imaged area, may not be useful when the assumption that the backscattered change of phase is only due to Δz is violated (in higly vegetated areas, for example). A further error source is due to atmospheric propagation effects and the interactions with the ionosphere (Franceschetti and Lanari 1999, Massonnet and Feigl 2000): heavy rain, clouds or tropospheric layers with different refraction index can cause additional phase contribution which in turn could severely affect information on Δz.

3. Case study: feasibility of the DIFSAR technique with ERS tandem images

This section shows a case study performed on a test-site located in the Matese complex (Southern Italy), affected by complex regional stress fields and significant variations of the deformation fields, due to stress fields acting in the southern and mid-northern parts of the Apennines (Hippolyte *et al.*, 1994, Lavecchia, 1988, Ponte 1997).
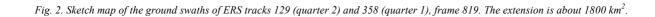
The availability of several ERS-1/ERS-2 tandem acquisitions over the Sannio-Matese area during the last years has greatly improved the possibility of obtaining highly correlated SAR datasets, due to the one-day revisiting period. The constraints on the baseline component perpendicular to the line of sight, $B_\perp$, lock the critical values of $|B_\perp|$ in the range from 70 to 130 m, for efficient phase unwrapping and small baseline decorrelation (Li and Goldstein, 1990, Prati and Rocca, 1990): the tandem pairs with such values of $B_\perp$ are reported in Tab. 2. Perpendicular baselines greater than this critical value induce high spatial decorrelation, degrade severely the coherence (defined later in Eq. (15)) and adding noise to the phase difference information. Fig. 2 depicts the imaged area.

Table 2. ERS-1/ERS-2 tandem pairs analyzed and correspondent perpendicular baseline component estimates.

Acquisition date	Orbit numbers	$B_\perp$ (m)
May 7-8, 1996	25167(ERS-1) / 5494 (ERS-2)	122
May 23-24, 1996	25396 (ERS-1) / 5723 (ERS-2)	81
June 27-28, 1996	25897 (ERS-1) / 6224 (ERS-2)	78

Top left	41°33' N – 14°04' E
Top right	41°33' N – 14°52' E
Bottom left	41°01' N – 14°04' E
Bottom right	41°01' N – 14°51' E

Fig. 2. Sketch map of the ground swaths of ERS tracks 129 (quarter 2) and 358 (quarter 1), frame 819. The extension is about 1800 km².

3.1 Interferometric SAR processing

Single-look complex (SLC) images, processed by ESA/ESRIN, have been acquired in the framework of a project developed in the last few years (Ponte 1997). The average dimensions of each frame are 15000 lines of 2200 range samples. Fig. 3a shows, as an example, one of these images, multilooked by a factor 5 in the azimuth direction in order to get a square pixel (about 20x20 m^2), and mirrored about its horizontal axis, to obtain a north-south image.
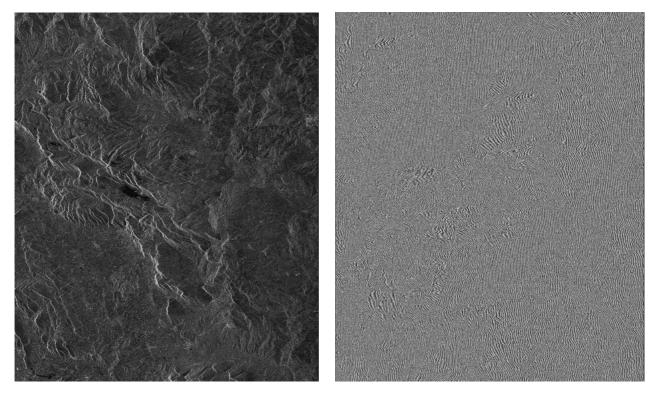

Fig. 3.(a) ERS- 1 image of the Sannio-Matese area (orbit 25167, frame 819, track 129) (© ESA 1996); (b) 5-look interferogram obtained from the ERS tandem pair of May 7-8, 1996 (see Tab.2). The image dimensions are 2400x2400 pixels.

The Matese Chain and the Matese Lake are well visible on the central portion of the frame, and a division of the massif into three blocks with respect to the NW-SE-oriented Matese Lake-Letino structure is suggested by the radar image. The capability of producing DEMs on different 10x10-km^2 subareas of the test-site has already been accomplished by using November 1995 and February 1996 ERS tandem pairs and implementing an efficient end-to-end procedure, from geometric registration to baseline components estimation from the propagated state vectors available in each SLC header file (Rufino *et al.* 1996).

The available conventional SAR images have successively been processed in order to get the single-difference interferograms. In the following is reported the logic flow of the operations performed for fringe maps generation:
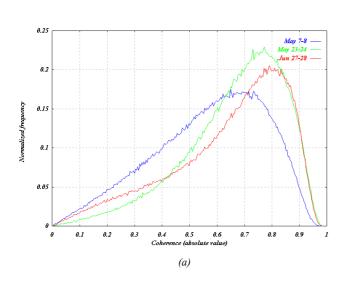
- Coarse registration by rigid translation. A number of visually-inspected bright points common to both images has been used to cut non-overlapping areas, obtaining a residual misregistration of the order of three pixels.
- Fine registration by localization in each 512x256 pixel subset of the brightest point target as a Ground Control Point (GCP). The evaluation of the pixel shifts to be applied for registration has been performed by 10-time oversampling each subset (cubic B-splines have been used for interpolation) and cross-correlating the GCP amplitudes. The average number of suitable GCP, after elimination of poorly correlated subsets and inconsistent shifts derived from the procedure, has found to be from 150 to 200, depending on the size of the images: such an high number, as compared to past experience with 3-day ERS-1 pairs (Moccia *et al.*, 1994), can take account for possible nonlinearities due to the pointing geometry and/or attitude differences.
- Coregistration by means of bicubic polynomials, whose coefficients have been computed with least-square approximations, by using as input the sub-pixel shifts. As a remark, we noted that the range and azimuth residual shifts are quite constant for the three pairs analyzed, with a slight increase of azimuth sub-pixel displacement from near to far range, probably due to small differences in attitude (i.e. pointing geometry) between the two passes, or to non perfectly parallel orbits.
- Complex product between the coregistered SLC images (the second one being complex conjugated). No common spectral band filtering before computation of the fringe map has been performed, thus leaving a residual baseline decorrelation.

- Coherent multilook for coherence enhancement and maximum likelihood estimation of the interferometric phase (Werner *et al.*, 1992).

As can be seen in Fig. 3b, the obtained interferograms show good quality of the fringes, and comparatively small decorrelated areas, due to the short (1-day) temporal baseline. Fringe quality has been evaluated by means of the correlation coefficient γ:

$$\gamma = \frac{\left\langle p_{i1} p_{i2}^{*} \right\rangle}{\sqrt{\left\langle p_1 \right\rangle^2 \left\langle p_2 \right\rangle^2}} \tag{15}$$

where * denotes complex conjugation, p_{i1} and p_{i2} are homologous pixels in the two co-registered images, and $\langle\rangle$ is the expectation operator. Fig. 4a shows coherence histograms of the multilooked interferograms, and Fig. 4b shows the coherence image relative to the June 27-28, 1996 pair. Fig. 4b is a color-composite image obtained by superimposing (red and blue channels) the interferogram to the coherence map, in order to visually inspect areas of low coherence. Finally, Table 3 reports a statistical characterization of γ.
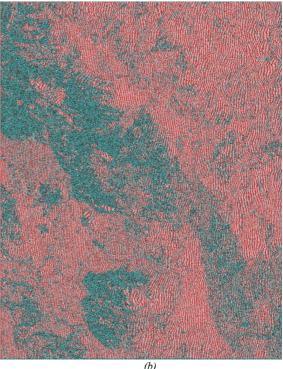

(a)

(b)

Fig. 4. (a) Coherence histograms of the three tandem pairs selected; (b) Composite image of coherence+interferogram .

Table **3**. Coherence statistics.

Tandem pair	Mean	St. dev.
May 7-8, 1996	0.55	0.21
May 23-24, 1996	0.59	0.05
June 27-28, 1996	0.63	0.04

The Matese Chain, a densely vegetated mountainous area (descending diagonally from top left to bottom right in the image of Fig. 4), shows, as expected, low coherence, whereas flat areas and bare soil exhibit larger correlation. With respect to the corresponding SAR images (Fig. 3a), some ground features are more identifiable: for example, rivers Volturno and Calore are clearly visible in the lower left part. The good coherence values found are a consequence of the reduced temporal gap between the two observation, and it is expected that stripping off mountainous areas and zones in which layover due to high slopes occur could even increase the average coherence. As a remark, layover areas reduce the possibility of efficient phase unwrapping for DEM generation, as shown by analyses conducted on different pairs of the illuminated area by Rufino *et al.*, 1996. Temporal decorrelation shows changes in land use, vegetation cover and moisture, as well as roughness and hydro-meteorological changes.

3.2 DIFSAR feasibility study on the available ERS interferometric couples

Since the test-site is a densely vegetated area, with little urbanization and sparse bare-soil regions, the loss of coherence is significantly high even after few days, a constraint which gives non-tandem data of the area (e.g. ERS-1/ERS-1, ERS-2/ERS-2 pairs, or ERS-1/ERS-2 passages with more than 1-day separation) a relatively low information content, and limits heavily the DIFSAR approach to these categories of soil. This section will justify quantitatively this observation, nonetheless showing the possibility of obtaining DIFSAR maps on some non-vegetated areas present in the illuminated scene. The investigation has been conducted on two tandem pairs, namely, the May 23-24 and the June 27-28 couples (see Tab. 2), chosen because of their suitable $B_\perp$ values (81 and 78 m for the tandem pairs, about 80 m between non-tandem observations). Fig. 5 shows the coherence histograms obtained from processing two non-tandem combinations of the available SLC products. The average values found for γ are 0.28 and 0.27 for the ERS-1/ERS-2 and the ERS-2/ERS-2 pairs, respectively, with standard deviation of 0.02.The low γ-values are due to the wide temporal baseline (34 and 35 days respectively) and to possible cultivation in vegetated areas (harvesting).
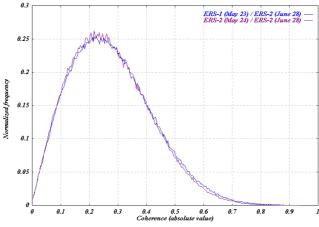

Fig. 5. Coherence histograms of the analyzed non-tandem pairs.

As a result, fringes are visible only in little portions of the image. Fig. 6 shows such an area, corresponding to Mount La Gallinola (in the Matese Mount Maggiore unit, direction NE with respect to the Matese Lake, see Fig. 2), a non-vegetated site formed by milestones, clay and marl. Poor-quality fringes are visible on a bare-soil area, which exhibits an average coherence of 0.4. The dimension of this subset are 128x128 pixels, and 5-look coherent summing has been applied in the azimuth direction.
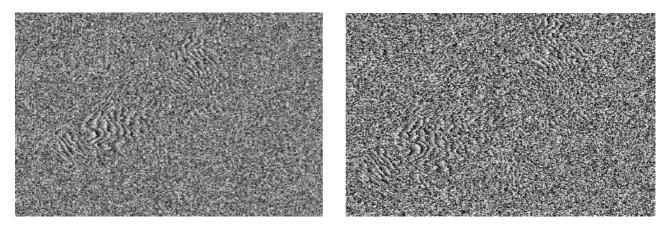

Fig. 6. Portion of the interferograms obtained from ERS-1 (May 23)/ERS-2 (June 28) images (left) and ERS-2(May 24)/ERS-2 (June 28) pairs (right).

The lack of large and representative high-coherence areas seems to reduce the impact of change detection by means of DIFSAR data. Nonetheless, the presence of a number of corner reflectors (CR) deployed on the test-site could allow us to obtain a correct phase sampling on a small subset of high-coherence points (the point target images), whereas GPS measurements on the absolute CR locations should permit the reconstruction of the absolute phase of each reflector, and, as a consequence, the possibility of detecting surface changes in the vicinity of the CRs. In a first attempt of this procedure, the identification of the CR responses in the images and the extraction of geometric and radiometric image quality parameters (range and azimuth resolutions, integrated and peak sidelobe ratio (ISLR, PSLR)) by means of

appropriate algorithms (Moccia *et al.*, 1994b, Rufino *et al.*, 1996), allowed us to obtain a set of control points with good phase quality. Retrieving the relative phase of the CRs was not much successful, though, since the CRs are immersed in low-coherence areas.

4. Concluding remarks

The rationale of differential interferometric SAR technique has been presented in this work, together with a sensitivity analysis and a quick exploration of the limits inherent to this methodology. A feasibility study on the applicability of spaceborne DIFSAR data for change detection has been applied to the analysis of ERS tandem pairs of the Sannio-Matese mountain chain, showing critical dependence on the scene coherence and on the temporal decorrelation. Surface change detection seems to be difficult on vegetated zones, where temporal decorrelation effects are undistinguishable from displacement-related effects. The technique (through the use of spaceborne inteferometric couples) has been found to be potentially applicable only in small subsets of the analyzed scene, namely to little or not vegetated areas, due to the very long temporal baselines and the high local scene changes not attributable to crustal deformations, even if the single-difference interferograms showed good-quality fringes and relatively high coherence. This indicates potential suitability of the technique to displacement mapping of planetary bodies, since recoverable ground displacements are critically dependent on the "stability" of the imaged area. Missions with increased repeat-track interferometric capability are foreseen as a crucial step towards optimization of interferometric data, in terms of selection of suitable temporal baselines (dependent on the time scale of the crustal dynamics to be investigated), look angles (in order to extract different displacement components), coverage and revisit time, data accessibility. Possible future development of the work presented here will concern the following points:

- Exploiting phase information derived from the installed CRs for effective phase unwrapping and DEM generation. Computer simulation of the SAR system will allow us to create artificial fringe maps, generate the reference function necessary to compress the raw data and enhance the interferogram coherence. The simulation technique has been successfully applied on SIR-C/X-SAR data (Ponte and Moccia, 1995), which shown better resolutions when compressed with the simulated 2D impulse response function.
- Correlation between GPS measurements and differential interferometry, and synergistic use of multi-source imagery for geological analysis.
- Refinement of baseline estimation methods and orbital modeling, for improvements in quality of interferometric processing.
- Development of local-scale seismo-tectonical models based on DIFSAR data.

5. References

Barbano MS, Egozcue JJ, Fernandez G, Kijko A, Lapajne J, Mayer-Rosa D, Schenk V, Schenkova Z, Slejko D, Zonno G (1989) Assessment of seismic hazard for the Sannio-Matese area of Southern Italy - A summary. Natural Hazard, **2**, pp. 217-228

Crocetto N, Ponte S (2001) A 3-D imaging topographical application of interferometric Synthetic Aperture Radar (SAR) data: Digital Elevation Model (DEM) extraction. Workshop 2001 Italy-Canada "3-D Digital Imaging and Modeling Application of: heritage, industry, medicine & land", April 3-4, 2001, Padua, Italy

Franceschetti G, Lanari R (1999) Synthetic Aperture Radar processing. CRC Press, chap. 4

Gabriel AK, Goldstein RM, Zebker HA (1989) Mapping small elevation changes over large areas: differential radar interferometry. Journal of Geophysical Research, **94**, No. B7, pp. 9183-9191

Hippolyte JC, Angelier J, Roure F (1994) A major geodynamic change revealed by Quaternary stress patterns in the Southern Apennines (Italy). Tectonophysics, **230**, pp. 199-210

Lavecchia G (1988) The Thyrrenian-Apennines system: structural setting and seismotectogenesis. Tectonophysics, **147**, pp. 263-296

Li FK, Goldstein RM (1990) Studies of multi-baseline spaceborne interferometric synthetic aperture radars. IEEE Trans. Geosc. Rem. Sens., **1**, pp. 88-97

Madsen SN, Zebker HA (1998) Imaging Radar Interferometry. In: Henderson FM, Lewis AJ (Eds.) Principles and Applications of Imaging Radar. John Wiley and Sons, Inc., pp. 359-380

Massonnet D (1993) Displacement Fields Mapped by Radar Interferometry. Proceedings of the CRCM '93, Kobe, Japan, pp. 139-145

Massonnet D, Vadon H and Rossi M (1996) Reduction of the need for phase unwrapping in radar interferometry. IEEE Trans. Geosc. Rem. Sens., **34**, pp. 489-497

Massonnet D, Feigl KL (2000) Radar interferometry and its application to changes in the Earth's surface. Rev. Geophys. Vol. 36, No. 4, pp. 441-500

Moccia A, Esposito S and D'Errico M. (1994) Height measurement accuracy of ERS-1 SAR interferometry. EARSeL Adv. Rem. Sens., **1**, pp. 94-108

Moccia A, Vetrella S and Ponte S (1994b) Passive and active calibrators characterization by using a spaceborne SARsystem simulator. IEEE Trans. Geosc. Rem. Sens., **32**, pp. 715-721

Ponte S, Moccia A (1995) Validating a spaceborne SAR simulator by using SIR-C/X-SAR data. 46th IAF Congress, Oslo, Norway. Paper IAF-95-B.6.03

Ponte S (1997) ERS Tandem Data for Earthquake Prediction: Preliminary Results. Proceedings of the 3rd ERS Symposium on Space at the service of our Environment, Florence, Italy, ESA-SP-414, Vol. 3, pp. 499-506

Prati C, Rocca F (1990) Limits to the resolution of elevation maps from stereo SAR images. *Int. J. Rem. Sens.*, **11**, pp. 2215-2235

Prati C, Rocca F, and Monti Guarnieri A (1993) SAR interferometry experiments with ERS-1. Proceedings of the 1st ERS-1 Symposium, Cannes, France, pp. 211-218

Rosen PA, Hensley S, Joughin JR, Li FK, Madsen SN, Rodriguez E, Goldstein RM (2000) Synthetic Aperture Radar Interferometry. Proceedings of the IEEE, Vol. 88, No. 3, pp. 333-381

Rufino G, Moccia A, Esposito S (1996) DEM generation by means of ERS tandem data. ESA Workshop on Applications of ERS SAR interferometry (FRINGE 96), Zurich, Switzerland, Sep. 30-Oct. 2, 1996.

Siro L, Slejko D (1989) Different approaches to the seismic hazard of Sannio-Matese (Southern Italy). Natural Hazard, **2**, pp. 329-348.

Vadon H, Sigmundsson F (1997) 1992–1995 crustal deformation at Mid-Atlantic ridge, SW Iceland, mapped by radar interferometry. Science, v. 275, pp. 193–197

Werner CL, Goldstein RM, Rosen P, and Zebker HA (1992) Techniques and applications of SAR interferometry for ERS-1 topographic mapping, slope measurement and change detection. Proceedings of the 1st Workshop ERS-1 FRINGE Working Group, ESA/ESRIN, pp. 11

Zebker HA and Villasenor J (1992) Decorrelation in interferometric radar echoes. IEEE Transactions on Geoscience and Remote Sensing, Vol. 30, pp. 950-959

Zebker HA, Werner CL, Rosen PA and Hensley S (1994). Accuracy of Topographic Maps Derived from ERS-1 Interferometric Radar. IEEE Transactions on Geoscience and Remote Sensing, Vol. 32, pp. 823-836